Environmental Science & Technology

Article

pubs.acs.org/est

Effect of Strong Acid Functional Groups on Electrode Rise Potential in Capacitive Mixing by Double Layer Expansion

Marta C. Hatzell,[†,∥] Muralikrishna Raju,[‡] Valerie J. Watson,[§] Andrew G. Stack,[⊥] Adri C. T. van Duin,[†] and Bruce E. Logan*[,§]

[†]Department of Mechanical Engineering, [‡]Department of Physics, [§]Department of Civil and Environmental Engineering, The Pennsylvania State University, University Park, Pennsylvania 16802, United States

[⊥]Geochemistry and Interfacial Sciences Group, Chemical Sciences Division, Oak Ridge National Laboratory, Oak Ridge, Tennessee 37831, United States

Supporting Information

ABSTRACT: The amount of salinity-gradient energy that can be obtained through capacitive mixing based on double layer expansion depends on the extent the electric double layer (EDL) is altered in a low salt concentration (LC) electrolyte (e.g., river water). We show that the electrode-rise potential, which is a measure of the EDL perturbation process, was significantly ($P = 10^{-5}$) correlated to the concentration of strong acid surface functional groups using five types of activated carbon. Electrodes with the lowest concentration of strong acids (0.05 mmol g^{-1}) had a positive rise potential of 59 ± 4 mV in the LC solution, whereas the carbon with the highest concentration (0.36 mmol g^{-1}) had a negative rise potential (−31 ± 5 mV). Chemical oxidation of a carbon (YP50) using nitric acid decreased the electrode rise potential from 46 ± 2 mV (unaltered) to −6 ± 0.5 mV (oxidized), producing a whole cell potential (53 ± 1.7 mV) that was 4.4 times larger than that obtained with identical electrode materials (from 12 ± 1 mV). Changes in the EDL were linked to the behavior of specific ions in a LC solution using molecular dynamics and metadynamics simulations. The EDL expanded in the LC solution when a carbon surface (pristine graphene) lacked strong acid functional groups, producing a positive-rise potential at the electrode. In contrast, the EDL was compressed for an oxidized surface (graphene oxide), producing a negative-rise electrode potential. These results established the linkage between rise potentials and specific surface functional groups (strong acids) and demonstrated on a molecular scale changes in the EDL using oxidized or pristine carbons.

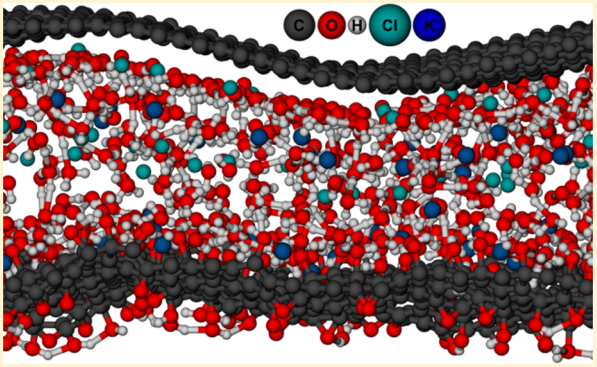

INTRODUCTION

Between 0.8 and 2.6 TW of power could be captured globally at estuaries through the natural mixing of sea and river water.[1,2] Capacitive mixing based on double layer expansion (CDLE), is an electricity-producing salinity gradient energy (SGE) technology that can harvest mixing energy using capacitive electrodes. Current competing pilot phase SGE technologies, pressure-retarded osmosis (PRO), and reverse electrodialysis (RED), require the use of membranes, which increases capital costs.[2−13] CDLE utilizes only low-cost activated carbon electrodes, potentially making CDLE the most sustainable conversion technique available for extracting energy from natural mixing processes.[14−21]

CDLE is the reverse of an emerging desalting technique termed capacitive deionization (CDI).[22−26] Energy is used in CDI to extract ions from a concentrated salt solution using supercapacitor-based electrodes, whereas energy can be produced using CDLE from the mixing of high and low salt concentration solutions. Energy extraction with CDLE takes place through four steps (Figure 1). Initially, electrodes are placed in a high salt concentration (HC, e.g., seawater), and they spontaneously charge (zero-charging), although charge can be increased using an external power supply (force-charging)[15−17,27,28] (step 1). Zero-charging is favored because this alleviates the need for an initial investment of energy into the system, and there is minimal charge leakage. Once this surface charge is established, the electrodes are placed in an open circuit (no external load), and a low concentration solution (LC, e.g., river water) displaces the HC solution. The change in concentration results in a perturbation of the electric double layer (EDL) on each electrode. The change in the EDL thickness, typically evaluated in terms of changes in the Debye length (λ), increases the potential drop through the diffuse portion of the EDL [$\varphi^{\pm}_{EDL} = f(\lambda)$], elevating the whole cell potential (φ_{cell}) (step 2). The capacitive electrodes are then discharged (at the higher potential), and energy is harvested through an external circuit (step 3). The cycle is completed

Received: September 10, 2014
Revised: October 25, 2014
Accepted: November 3, 2014
Published: November 3, 2014

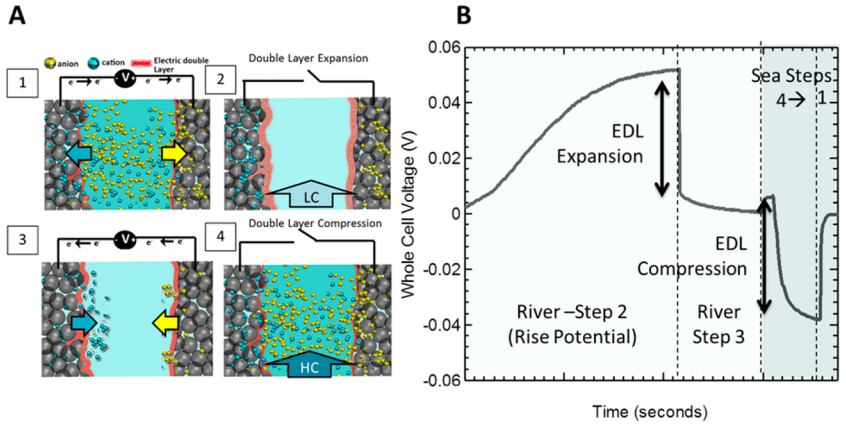

Figure 1. (a) Four-step capacitive mixing based on double layer expansion process. Step 1: electrodes charged in HC. Step 2: under open circuit, LC replaces HC solution, causing the EDL to expand (generating energy). Step 3: electrodes discharged at a higher potential (energy harvesting). Step 4: under open circuit, HC replaces LC, compressing the EDL. (b) Typical voltage response curve during a CDLE cycle with LC steps (2, EDL expansion; 3, discharge) shaded in light blue, and HC steps (4, EDL compression; 1, charge shaded in dark blue.

when HC displaces the LC under open circuit (fixed surface charge) conditions, compressing the EDL (step 4).[15]

The extent of the EDL expansion and material capacitance (C) dictate how much energy is generated during the CDLE process [$E_{CDLE} = (1/2)C(2\varphi_{EDL})^2$]. From the Poisson–Boltzmann equation and the Gouy–Chapman–Stern (GCS) model, the potential distribution in the diffuse portion of the EDL is

$$\varphi_{EDL} = \frac{L\sigma}{\epsilon_0\epsilon_r} = \frac{2k_bT}{e}\sinh^{-1}\left(\frac{\sigma}{\sqrt{8C_sN_A\epsilon_0\epsilon_rk_bT}}\right) \quad (1)$$

where k_b is the Boltzmann constant; T, the temperature; e, the electron charge; σ, the surface charge density; C_s, the salt concentration; N_A, Avogadro's constant; ε_0, the electric constant; ε_r, the relative dielectric constant; and L, the EDL effective thickness. The potential distribution (φ_{EDL}) increases as the surface charge density (σ) increases and the solution concentration decreases. During "zero-charging", the material properties dictate the surface charge density, whereas with "force-charging" the external power supply provides the surface charge density. Methods that increase the activated carbon's intrinsic charge density are needed to capture a significant amount of energy through the "zero-charging" method.

From the GCS model, an individual electrode operated with seawater and river water at the electrode's spontaneous potential could approach $\varphi_{EDL} \approx 60-90$ mV ($\varphi_{cell} = 2\varphi_{EDL}$). In practice, individual electrodes have approached the theoretical predictions, but the whole cell potential has not. The whole cell potential has remained low, typically between $\varphi_{cell} \approx -30$ and 30 mV.[15−18] This is because each individual electrode's rise potential is similar if the electrodes (positive and negative) have the same material properties. The low rise potentials also often have been attributed to operational concerns, such as incomplete solution removal, or charge leakage. To avoid this, it has been shown that materials with dissimilar rise potentials can be paired together to increase the whole cell voltage.[14,15] Ideally, the greatest whole cell potential rise occurs when one electrode decreases in potential ($\Delta\varphi^{\pm} < 0$) and the other increases in potential ($\Delta\varphi^{\pm} > 0$) when exposed to an LC solution. Through the use of electrodes with the most dissimilar rise potentials, the whole cell potential has approached $\varphi_{cell} \approx 100$ mV.[15] Although many different carbons have been examined in CDLE cells for the rise potentials, the physical and chemical characteristic that promote more positive or negative rise potentials have not been well explored.

The objective of this study was to examine the relationships between activated carbon chemical, physical, and electrochemical properties and the voltage rise (energy generation phase) that occurs in a CDLE cycle. It was previously shown that the rise potential was related to the point of zero charge (PZC) of different types of carbonaceous materials,[15] but the specific functional groups responsible for these differences were not explored. We hypothesized that the abundance and type (weak versus strong) of acid groups on the carbon surface were primarily responsible for the different behavior of the carbon materials.

To examine the specific role of carbon surface chemistry on the rise potential, activated carbons (ACs) that were derived from five different precursor materials were characterized using potentiometric titrations to quantify the concentration of acidic surface functional groups.[29] The materials were further examined in terms of their electrochemical (capacitance) and physical (pore size distribution, and total surface area) properties. The voltage rise ($\Delta\varphi^{\pm} > 0$) or fall ($\Delta\varphi^{\pm} < 0$) of each material was determined at its spontaneous potential. To demonstrate the importance of acid functional groups, we oxidized one of the carbons (using nitric acid) to show that this would alter the rise potential in a predictable direction. We measured the resulting whole cell potentials that could be produced using carbons with these different concentrations of surface acid groups in capacitive mixing tests based on a "zero-charging" CDLE process. Molecular dynamics and metadynamics simulations were performed using an idealized system to show that the responses of the EDL on plain carbon (pristine graphene) were different from those on a carbon surface containing a high abundance of oxygen groups (graphene oxide). This linkage between the specific surface chemistry and rise potentials has not previously been examined through both experimental and simulation approaches.

MATERIALS AND METHODS

Capacitive Mixing System. The CDLE device was manufactured from antistatic clear cast acrylic (McMasterCarr, IL). The end plates (5.1 × 5.1 × 0.95 cm) and a middle chamber (5.1 × 5.1 × 0.25 cm) were machined. Each end plate

had a 0.64 cm hole drilled and tapped so that a polypropylene tube fitting (0.64 cm tube o.d. × 0.64 cm male pipe) could be screwed into the end plate. Fine extruded graphite rods (0.64 cm diameter, Graphitestore.com, Inc.) were fitted into the polypropylene tube fitting and sealed using Loctite epoxy (McMasterCarr, IL). The graphite rods served as the current collector for the capacitive electrodes. The middle chamber was hollowed out, and this served as the flow cell (empty bed volume ∼2 mL). Tube fittings were glued to the top and bottom of the middle chamber, allowing for flow into and out of the cell. A reference electrode (Ag/AgCl +0.205 versus SHE) (BASi, West Lafayette, IN) was placed in the middle chamber to measure individual electrode potentials.

Electrode Preparation, Treatment, and Characterization. Capacitive electrodes were prepared from five commercially available activated carbon powders based on different precursor materials: peat (SX+) (Norit, USA), coconut shell (YP50, Kuraray Chemical, Japan), phenolic resin (RP-20, Kurraray Chemical, Japan), bituminous coal (BC, Carbon Resources, USA), and hardwood (HRD, MeadWestvaco, USA). To demonstrate that a carbon rise potential could be modified by chemical oxidation, YP50 was treated (YP50 ox) with nitric acid (0.5 M, Sigma-Aldrich, St. Louis MO) for 12 h.

Capacitive electrodes were prepared through combining the AC powder with 10 wt % polyvinylidene fluoride (Sigma-Aldrich, St. Louis MO). The mixture was homogenized with a sonifier in 2 mL of dimethylformamide (Sigma-Aldrich, St. Louis MO), and the slurry was cast onto graphite rods (∼3.2 mg cm^{-2}). Electrodes were dried overnight, washed with ethanol, and then soaked in 0.5 M sodium chloride before use in the CDLE system.

Cyclic voltammagrams (CVs) of each electrode were collected using a potentiostat (Biologic VMP-3, USA). The electrodes were scanned from 0 to 0.5 V at 2, 5, 10, 20, 50, and 100 mV s^{-1}, and the capacitance was calculated by

$$C_{sp} = \frac{2}{\Delta U} \cdot \frac{\int i dU}{\nu \cdot m} \tag{2}$$

where ΔU is the width of the voltage scan; i, the discharge current; U, the voltage; ν, the scan rate; and m, the mass of carbon on one electrode. Electrode properties for surface area, pore volume distribution, and strong acid surface functional groups were derived from experimental data previously collected to study oxygen reduction by these activated carbons.[29]

Spontaneous Potential Measurements. The spontaneous potential of each electrode was obtained through stepping the whole cell voltage from 0 to 1 at 0.2 V increments, where each voltage was held constant for 10 min to ensure steady conditions. The positive, negative, and whole cell voltage was monitored with Ag/AgCl reference electrodes. Step voltages were run three times to ensure repeatability. The potential of the individual electrodes measured at 0 V corresponded to the electrode's spontaneous potential.

Gouy−Chapman−Stern Model. The individual electrode potentials in different solutions ($\varphi^{\pm}_{LCzc/HC}$) and the resulting electrode potential rise or fall ($\Delta\varphi^{\pm} = \varphi^{\pm}_{LC} - \varphi^{\pm}_{HC}$) were estimated using GCS theory (eq 1).[14] These calculations produced curves of rise/fall potentials that were used to evaluate CDLE performance.[15] The vanishing point, defined as the zero-rise potential, differed on the basis of the solution concentration and the material properties of the activated carbons. We expected that the vanishing point would occur at the material's point of zero charge so that it could be obtained using the potentiometric titration data for each carbon (Supporting Information (SI) Figure S1).

Capacitive Mixing Performance. Capacitive mixing cycle tests were conducted to evaluate the whole cell potential and individual electrode potential rise with carbons with different surface chemistries when solutions were changed. The salt solutions were 0.5 M NaCl (HC) and 0.011 M NaCl (LC). These salt solutions were continuously pumped (peristaltic pump, Cole Parmer, IL) through the test cell at a flow rate of 5 mL min^{-1}. During energy extraction tests with the HC solution, the electrodes were connected to a 10 Ω resistor and charged to ∼0.0 V, then the LC solution was flushed through the cell. When the potential rise reached a plateau, the electrodes were discharged through a 100 Ω resistor until the whole cell reached ∼0.0 V. The HC was then pumped through the cell, and this cycle was repeated five times to ensure repeatability.

Molecular Dynamics (MD) Simulations. ReaxFF molecular dynamics (MD) simulations were used to calculate changes in EDL thicknesses that would occur during capacitive mixing tests with HC or LC solutions. ReaxFF reactive force field calculations were implemented using the ADF computational chemistry package.[30] A detailed description of the ReaxFF reactive force field method is given in van Duin et al.[31] and Chenoweth et al.[32] In the ReaxFF reactive force field, the total (system) energy is given by

$$E_{system} = E_{bond} + E_{val} + E_{tors} + E_{over} + E_{under} + E_{lp} + E_{vdWaals} + E_{coulomb} \tag{3}$$

where E_{bond} are the bond energies; E_{val}, the valence-angle energies; E_{tors}, the torsion-angle energies; E_{over}, the energy to penalize overcoordination of atoms; E_{under}, the energy to stabilize under-coordination of atoms; E_{lp}, the lone-pair energies; $E_{coulomb}$, the nonbonded Coulomb energies; and $E_{vdWaals}$, the nonbonded van der Waals interactions. ReaxFF uses a bond order/bond energy relationship, which allows for bond formation and bond dissociation during molecular dynamics (MD) simulations. The bond orders obtained from interatomic distances are updated at every MD or energy minimization step. All connectivity dependent interactions (e.g., valence-angle and torsion-angle energies) are bond-order-dependent, and therefore, energies and forces associated with these terms go to zero upon bond dissociation. ReaxFF calculates nonbonded interactions (van der Waals and Coulomb) between every atom pair, irrespective of their connectivity. Excessive short-range, nonbonded interactions are avoided by incorporating a shielding term in these interactions.

Pristine graphene (PG) sheets were used to model electrodes with a low concentration of strong acid functional groups, and graphene oxide (GO) sheets were used to model electrodes with a high concentration of strong acid functional groups (SI Figure S11). The atomic structure of GO sheets used in the simulations were obtained from MD studies by Bagri et al.[33] In these simulations, we used periodic slabs with dimensions 43.35 Å × 40.04 Å parallel to the surface to describe the electrodes. Water molecules, potassium, and chlorine atoms were placed in random configurations between the electrodes separated by 16 Å to represent the 2.4 M KCl solution, which was used as a representative high concentration solution in all simulations. The ReaxFF force parameters for C/H/O were the same as those used by Rahaman et al.[34] to describe graphene−water/

graphene oxide−water interactions, and the same as Rahaman et al.[35] for Cl/O/H to describe chloride−water interactions.

All MD simulations were performed in the canonical (NPT) ensemble, with a time step of 0.25 fs using the Berendsen thermostat with a coupling time constant of 100 fs and Berendsen barostat with a coupling time constant of 500 fs to control the temperature and pressure of the entire system. The system was energy-minimized with a convergence criterion of 0.25 kcal/Å and equilibrated in the canonical (NPT) ensemble for 50 ps at 300 K. The EDL thickness at the electrode surface for the HC electrolyte case was estimated from subsequent NPT simulations for 50 ps at 300 K. The potassium and chlorine ions that were not part of the EDL at the electrodes were removed manually to simulate the change from the HC to LC electrolytes. The resulting 0.9 M KCl solution was used as a representative LC solution in all simulations, and the EDL for this condition was obtained from MD simulations for 100 ps at 300 K. In these simulations the equilibration time was 50 ps, and the subsequent production run was 50 ps. Metadynamics was performed using version 1.3 of PLUMED[36] (called using a "fix" routine from lammps). Technical details are listed in the Supporting Information (SI).

RESULTS AND DISCUSSION

Surface Chemistry of the Carbon Electrodes. On the basis of potentiometric titrations, the concentration of acidic (Figure 2A) and oxygen-containing (SI Figure S1) functional groups was highest for the HRD sample and lowest for the SX+ (peat-based) carbon. The remaining carbons (YP50, BC, and RP20) contained intermediate concentrations of strong acid groups. The strong acid functional groups measured for the HRD sample were primarily oxygen-containing acids (e.g., phenolic, carboxylic, and lactonic).[29] Surface functional groups can act as a source of surface charge because the functional groups can undergo dissociation or protonation.[37] The HRD sample had the largest quantity of strong acid surface functional groups around the operating electrolyte's pH (e.g., pH = 7), whereas SX+ has the lowest concentration of functional groups at pH = 7 (SI Figure S2). The groups that could potentially dissociate or protonate at pH 7 were carboxylic acid groups, and thus, the concentration of these acid groups was of most interest relative to electrode rise/fall tests.

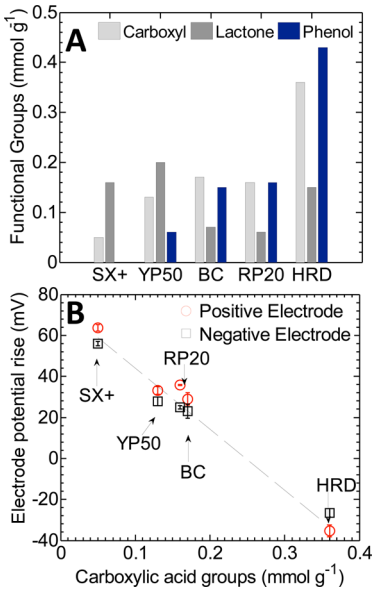

Figure 2. (a) Concentration of surface functional groups for various carbons tested and (b) the individual electrode ($\Delta\varphi^{\pm}$) potential rise as a function of the concentration of strong acid surface functional groups for different carbons.

Electrode Rise and Fall Measurements. The different rise potentials (positive and negative electrodes) obtained for the different carbons was found to be well correlated ($P = 10^{-5}$) with the concentration of carboxlic acid groups (Figure 2B). Carbons with high concentrations of oxygen-containing groups (HRD) caused both the positive and negative electrode potentials to decrease when a LC solution was added to the flow cell. Carbons with fewest groups had most negative potentials. By applying a linear regression to the individual electrodes' rise/fall potential curve, the projected maximum electrode rise potential could approach 75 mV (R^2 = 0.97; based on the y intercept). In all cases, when the positive and negative electrodes were the same, the whole cell potential rise was minimal, ±15 mV (SI Figure S3-A). This was due to the similar response of individual electrodes, as has been previously reported (SI Figure S3−B).[15] There was no correlation between the rise/fall potential magnitude and the micro, meso, or macroporous surface area or micro, meso, or macropore volume (SI Figure S4 and S5).

An increase in the concentration of strong acid groups of the carbons was consistent with the shift in the PZC. The SX+ and HRD carbons had PZCs that differed by nearly 5 pH units and ~300 mV (SI Figure S6-A). The GCS curves for HRD and SX+ were calculated by using the PZC as the vanishing point ($\Delta\varphi^{\pm}$ = 0). Both the positive and negative electrode rise/fall potentials for SX+ and HRD were in good agreement with those predicted using the GCS theory. When similar electrodes are used for CDLE, to establish a large potential difference between individual electrodes, the electrodes need to be pushed away from their spontaneous base potentials along the same GCS curve (SI Figure S6−B). With dissimilar electrodes (with different PZC), the system is able to operate on two GCS curves, which promotes a potential difference between each individual electrode and another, even at the whole cells' spontaneous base potential.[15] Furthermore, when one electrode's spontaneous base potential is greater than the PZC, and the other electrode's spontaneous base potential is below the PZC (as is the case with SX+ and HRD), it is expected that one electrode will rise and one electrode will fall as the solutions are altered, which is desired. When the electrodes with the two most dissimilar concentrations were examined (SX+ and HRD), the whole cell potential rise reached 86 ± 1.7 mV, with the SX+ as the positive electrode and the HRD as the negative electrode (SI Figure S7).

Producing Dissimilar Electrodes through Chemical Oxidation. The YP50 electrode was oxidized using nitric acid to increase the concentration of positive surface functional groups. This oxidation process, used for treatment of supercapacitors, is known to increase the concentrations of strong acid groups by 2−3 times, depending on the time and concentration of acid used.[38,39] Using the oxidized negative electrode (YP50 ox) with a nonoxidized positive electrode (YP50) increased the whole cell potential from 12 ± 1 to 53 ± 1.7 mV (Figure 3A). Ideally, the potential rise observed with the similar electrodes would be 0 mV. Here, the minimal (~10 mV) voltage rise can be attributed to slight variations among the individual film electrodes. Slight differences in the surface

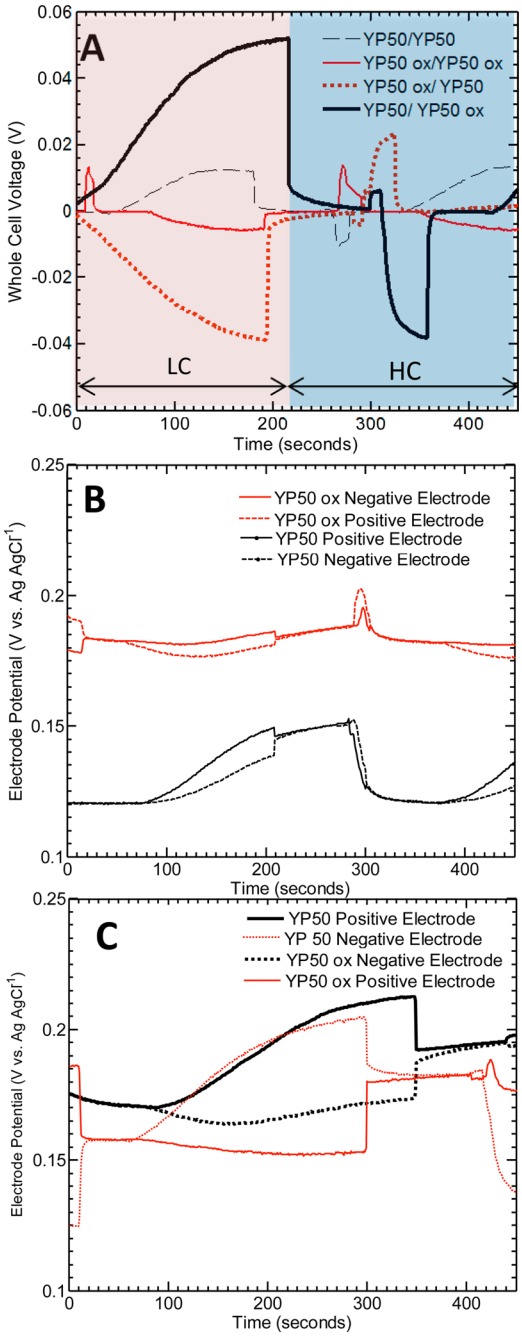

Figure 3. (a) Whole cell CDLE performance with similar and dissimilar electrodes YP50/YP50 ox,YP50 ox/YP50, YP50/YP50, and YP50ox/YP50 ox, (b) individual rise and fall potentials for similar electrodes (YP50/YP50 and YP50 ox/YP50 ox), and (c) individual rise and fall potentials for dissimilar electrodes (YP50/YP50ox and YP50 ox/YP50).

chemistry due to the presence of a contaminant or nonuniformity of the material, localized pH effects, or a nonhomogenous application of the binder in the electrode could all account for this small voltage rise. The increase with the dissimilar electrodes was due to the directional differences between the individual electrode rise potentials. The use of this dissimilar configuration produced a whole cell potential rise which was 3−10 times greater than that obtained using either of the similar-electrode configurations (YP50/YP50 or YP50ox/YP50ox) (Figure 3B). Chemical treatment reduced the rise potential of the YP50 from $\Delta\varphi^{+}_{YP50}$ = 46 ± 2 mV, to $\Delta\varphi^{-}_{YP50ox}$ = −6 ± 0.5 mV (YP50-ox, Figure 3B and C).

Treating activated carbons to alter surface functional groups may be more preferable than choosing materials with dissimilar concentrations of strong acid groups because this allows more control over material properties (e.g., exact functional groups, pore distribution, or surface area). YP50 is a typical activated carbon used for supercapacitors because it has a high surface area and a large concentration of micropores and, consequently, a high capacitance (SI Figure S8). On the basis of the energy equation $[E_{CDLE} = (1/2)C(2\varphi_{EDL})^2]$, if the voltage rise acquired through treatment methods can approach that of dissimilar materials, increasing the capacitance by 2 times (as is the case when YP50ox is used instead of the HRD sample) will double the amount of energy extracted from a CDLE cycle (SI Figure S9). Thus, the addition of chemical functionality through surface treatments, such as the oxidization process used here, is preferable to selecting materials on the basis of the rise potential alone because it ensures that the carbon will also have a high capacitance.

Theoretical Results: Evaluation of EDL Thickness. PG and GO sheets were examined as positive electrodes in MD simulations by assigning a net charge of 0.1*e* per atom, or as negative electrodes by assigning −0.1*e* per atom. In the absence of ions, the simulated charge distribution corresponds to a potential difference of 1.8 V between the electrodes.[40] The system is "force-charged" to be able to observe the formation of an EDL at the electrodes within the time-scale of our simulations. The formation of an EDL at the electrodes for the case that PG was the positive electrode and GO was the negative electrode, in the HC electrolyte case, is shown in Figure 4A. The ions that were not part of the capacitance or Stern layer (not adsorbed to the electrode) were removed manually to simulate the change from high- to low-concentration electrolyte (Figure 4B).

At equilibration, the EDL thickness at the PG electrode increased when changing from the HC to LC electrolyte, irrespective of whether PG was the positive electrode or negative electrode. The EDL thickness increased by 0.11 ± 0.05 Å when PG was the positive electrode, and 0.10 ± 0.05 Å when PG was the negative electrode. The GO electrode showed the converse behavior: the EDL thickness decreased on going from the HC to LC electrolyte, with the direction of this response (but not the magnitude) independent of whether GO was simulated as the positive or negative electrode in the cell. The EDL thickness decreased by 0.10 ± 0.06 Å when GO was the positive electrode and decreased by 0.17 ± 0.05 Å when GO was the negative electrode. The EDL expansion at PG produced a positive-rise electrode potential, and the EDL compression at GO produced a negative-rise potential at the electrode during the CDLE cycle. These simulation results were in agreement with the experimental observations that electrodes with a low concentration of strong acid functional groups showed a positive potential rise, and electrodes with a high concentration of strong acid functional groups showed a negative potential rise during the CDLE cycle, irrespective of whether they were the positive or negative electrode in the cell. A change in the EDL thickness of 0.10 Å corresponds to an electrode rise potential of 11.12 mV for the simulated charge distribution and is within the range of experimentally observed electrode rise potentials (cf. Figure 2).

To investigate the origins of the dissimilar EDL changes at the PG and GO electrodes, we performed metadynamics

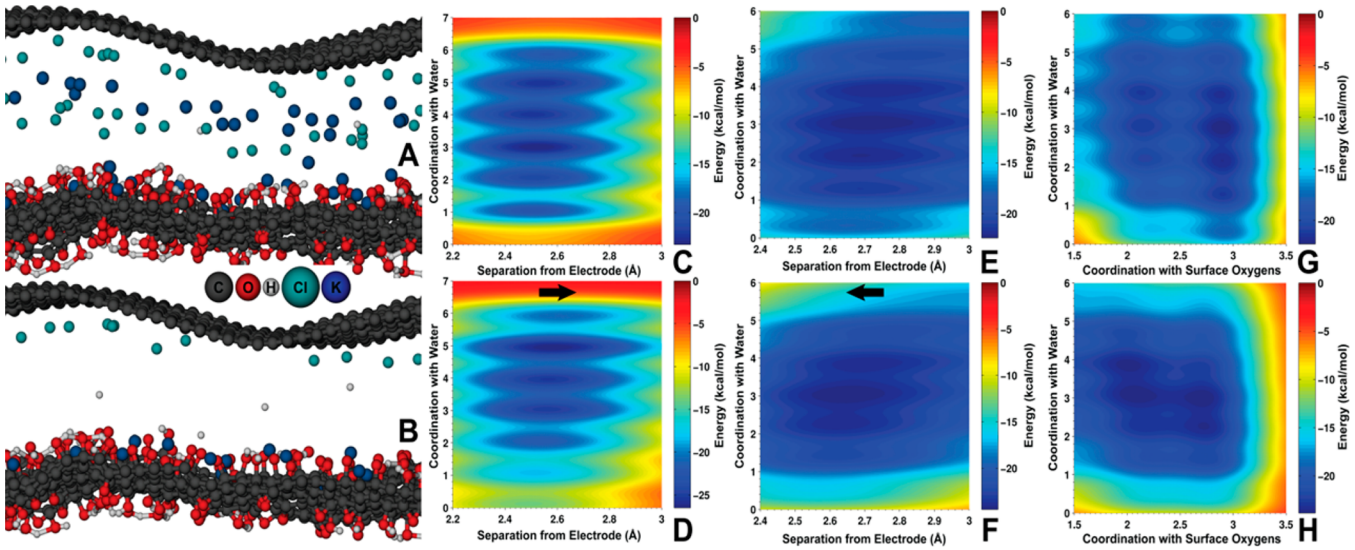

Figure 4. Snapshot from a MD simulation showing the electric double layer (EDL) in the (a) high concentration electrolyte and (b) low concentration electrolyte; the water molecules are not shown explicitly. Free-energy surface for adsorption of chlorine ion on the pristine graphene (PG) electrode as a function of separation from the electrode and coordination with water for the (c) high-concentration electrolyte and (d) low-concentration electrolyte when PG is the postive electrode in the cell. Free-energy surface for adsorption of potassium ion on the graphene oxide electrode as a function of separation from the electrode and coordination with water for the (e) high-concentration electrolyte and (f) low-concentration electrolyte when GO is the negative electrode in the cell. The arrows indicate the direction of shift of free-energy basins when changing from high- to low-concentration electrolyte. Free-energy surface for adsorption of potassium ion on the graphene oxide electrode as a function of coordination with surface oxygens and coordination with water for the (g) high-concentration electrolyte and (h) low-concentration electrolyte when GO is the negative electrode in the cell.

simulations to investigate the free-energy surface (landscape) of ions with the separation of ions from the electrode and solvation of ions in water as the collective variables (CVs). Details of the metadynamics methodology and free-energy surfaces (FESs) are given in the Supporting Information. Figure 4C−H are the reconstructed FESs as a function of the selected CVs obtained from the metadynamics simulations. In Figure 4C−H, we are primarily interested in the change in positions of free-energy minima (location of darkest blue color) when we go from a HC to LC electrolyte.

Figure 4C,D shows the free-energy surface of chloride ions near the PG electrode for the high-concentration electrolyte and low-concentration cases, respectively, when PG is the positive electrode in the cell. From these two figures, we observe that changing the HC to LC moves the position of minimum free-energy of the chloride ion farther away from the PG electrode (x axis) and that its coordination with water increased from 3 to 5 (y axis). In the HC electrolyte, the minimum free energy of the chloride ion is at a separation of 2.51 Å from the PG electrode; in the LC electrolyte, this increases to 2.59 Å. This suggests that in the LC electrolyte, because of the absence of surrounding ions, the chloride ions were stabilized by moving farther into solution and coordinating with more water molecules. This resulted in an EDL expansion, which would produce a positive potential rise at electrodes having a low concentration of strong acid functional groups.

With GO as the negative electrode, changing from the HC to LC concentration electrolyte moves the position of minimum free energy of the potassium ion closer to the GO electrode (x axis), and its coordination with water remained around 3 (y-axis) (Figure 4E,F). In the HC electrolyte, the minimum free energy of the potassium ion is at a separation of 2.73 Å from the GO electrode, and in the low concentration electrolyte, this decreases to 2.65 Å. At the GO electrode, ion coordination with surface oxygen atoms was also considered as a collective variable because the surface oxygen atoms could provide part of the solvation shell for the potassium ions near the GO electrode. We can note from SI Figure S10 that in the LC electrolyte, the potassium ion moves closer to the electrode, and at the same time, its coordination with surface oxygen atoms has decreased slightly from 2.9 to 2.7 (y axis).

The FES of potassium ions near the GO electrode is shown in Figure 4G,H as a function of coordination with surface oxygen atoms (x axis) and coordination with water (y axis). In the HC electrolyte, the free-energy minimum was produced when potassium was coordinated with three water and three surface oxygen atoms. In the LC electrolyte, the potassium ion had closely spaced free-energy basins at (3,3) as well as (2,4), with a barrier of 1.27 kcal mol^{-1} between the basins. This suggests that in the LC electrolyte, the potassium ion can move closer to the electrode and preserve its total coordination of 6. This would produce an EDL compression and thereby a negative potential rise at electrodes with a high concentration of strong acid functional groups.

The strong acid functional groups on the electrodes provide part of the solvation shell of the adsorbing ion, and in their presence, the adsorbing ion moves closer to the electrode in the LC electrolyte, producing a negative rise potential. In the absence of strong acid functional groups, the adsorbing ion moves away from the electrode in the LC electrolyte to increase its solvation in water, producing a positive rise potential. This results in the opposite rise potential trends on electrodes with low and high concentrations of strong acid function groups.

Outlook. CDLE represents a potentially clean, inexpensive, and sustainable method for extracting energy from salinity gradients, but energy recoveries need to be improved by increasing whole cell voltages. The concentration of strong acid

surface functional groups was shown here to strongly correlate with both the direction and magnitude of the individual electrode potential rise/fall. This indicates that carbons can be preselected to function as the positive or negative electrodes on the basis of the concentration of strong acid groups. However, the carbons best suited for CDLE must have high capacitance as well as dissimilar rise potentials. Thus, it may be more beneficial to chemically modify high capacitance carbons to obtain highly disparate concentrations of strong acid groups. A carbon with a high rise potential was transformed into a carbon with a low rise potential through chemical oxidation using a strong acid. Additional chemical treatments could be used to tune the type of functionality and the ideal concentration of acidic or basic functionality to improve the potential rise of both the positive and negative electrodes. Methods to chemically modify the carbons to have more positive rise potentials are as yet unidentified. ReaxFF simulations revealed that the rise and fall potential of individual electrodes could be attributed to the EDL expanding or compressing in the LC electrolytes. Additional MD simulations could provide guidance for producing the desired carbon chemistry.

■ ASSOCIATED CONTENT

Supporting Information

Activated carbon characterization (potentiometric titrations and cyclic voltammetry), capacitive mixing performance measurements, and molecular simulations. This material is available free of charge via the Internet at http://pubs.acs.org/.

■ AUTHOR INFORMATION

Corresponding Author

*Phone: +1 814 863 7908; fax: +1 814 863 7304; e-mail: blogan@psu.edu.

Present Address

[‖]George Woodruff School of Mechanical Engineering, Georgia Institute of Technology, Atlanta, GA 30332.

Notes

The authors declare no competing financial interest.

■ ACKNOWLEDGMENTS

This material is based upon work supported by the National Science Foundation Graduate Research Fellowship Program to M.C.H. under Grant No. (NSF) DGE1255832, and a grant from the King Abdullah University of Science and Technology (KAUST) (Award KUS-I1-003-13). A.C.T.V.D. and M.R. conducted reactive force field modeling with support from the Fluid Interface Reactions, Structures and Transport (FIRST) Center, an Energy Frontier Research Center funded by the U.S. Department of Energy, Office of Science, Office of Basic Energy Sciences. A.G.S. conducted metadynamics modeling with support from the Division of Chemical Sciences, Geosciences and Biosciences, Office of Science, Office of Basic Energy Sciences, U.S. Department of Energy.

■ REFERENCES

(1) Ramon, G. Z.; Feinberg, B. J.; Hoek, E. M. V. Membrane-based production of salinity-gradient power. *Energy Environ. Sci.* **2011**, *4* (11), 4423−4434.

(2) Weinstein, J. N.; Leitz, F. B. Electric power from differences in salinity: the dialytic battery. *Science* **1976**, *191* (4227), 557.

(3) http://www.statkraft.com/ (January 20, 2014).

(4) RED stack. http://www.redstack.nl/ (accessed May 21, 2014).

(5) Loeb, S. Production of energy from concentrated brines by pressure-retarded osmosis: I. Preliminary technical and economic correlations. *J. Membr. Sci.* **1976**, *1* (0), 49−63.

(6) Loeb, S.; Van Hessen, F.; Shahaf, D. Production of energy from concentrated brines by pressure-retarded osmosis: II. Experimental results and projected energy costs. *J. Membr. Sci.* **1976**, *1* (0), 249−269.

(7) Veerman, J.; Saakes, M.; Metz, S. J.; Harmsen, G. J. Reverse electrodialysis: A validated process model for design and optimization. *Chem. Eng. J.* **2011**, *166* (1), 256−268.

(8) Veerman, J.; Saakes, M.; Metz, S.; Harmsen, G. Reverse electrodialysis: evaluation of suitable electrode systems. *J. Appl. Electrochem.* **2010**, *40* (8), 1461−1474.

(9) Veerman, J.; de Jong, R. M.; Saakes, M.; Metz, S. J.; Harmsen, G. J. Reverse electrodialysis: Comparison of six commercial membrane pairs on the thermodynamic efficiency and power density. *J. Membr. Sci.* **2009**, *343* (1−2), 7−15.

(10) Veerman, J.; Saakes, M.; Metz, S. J.; Harmsen, G. J. Reverse electrodialysis: Performance of a stack with 50 cells on the mixing of sea and river water. *J. Membr. Sci.* **2009**, *327* (1−2), 136−144.

(11) Post, J. W.; Veerman, J.; Hamelers, H. V. M; Euverink, G. J. W.; Metz, S. J.; Nymeijer, K.; Buisman, C. J. N. Salinity-gradient power: Evaluation of pressure-retarded osmosis and reverse electrodialysis. *J. Membr. Sci.* **2007**, *288* (1−2), 218−230.

(12) Hatzell, M. C.; Logan, B. E. Evaluation of flow fields on bubble removal and system performance in an ammonium bicarbonate reverse electrodialysis stack. *J. Membr. Sci.* **2013**, *446*, 449−455.

(13) Hatzell, M. C.; Cusick, R. D.; Ivanov, I.; Zhu, X.; Logan, B. E. Comparison of hydrogen production and electrical power generation for energy capture in closed-loop ammonium bicarbonate reverse electrodialysis systems. *Phys. Chem. Chem. Phys.* **2014**, *16* (4), 1632−1638.

(14) Brogioli, D.; Ziano, R.; Rica, R.; Salerno, D.; Mantegazza, F. Capacitive mixing for the extraction of energy from salinity differences: Survey of experimental results and electrochemical models. *J. Colloid Interface Sci.* **2013**, *407*, 457−466.

(15) Brogioli, D.; Ziano, R.; Rica, R. A.; Salerno, D.; Kozynchenko, O.; Hamelers, H. V. M; Mantegazza, F. Exploiting the spontaneous potential of the electrodes used in the capacitive mixing technique for the extraction of energy from salinity difference. *Energy Environ. Sci.* **2012**, *5* (12), 9870−9880.

(16) Brogioli, D.; Zhao, R.; Biesheuvel, P. M. A prototype cell for extracting energy from a water salinity difference by means of double layer expansion in nanoporous carbon electrodes. *Energy Environ. Sci.* **2011**, *4* (3), 772−777.

(17) Brogioli, D. Extracting renewable energy from a salinity difference using a capacitor. *Phys. Rev. Lett.* **2009**, *103* (5), 058501.

(18) Rica, R. l. A.; Brogioli, D.; Ziano, R.; Salerno, D.; Mantegazza, F. Ions transport and adsorption mechanisms in porous electrodes during capacitive-mixing double layer expansion (CDLE). *J. Phys. Chem. C* **2012**, *116* (32), 16934−16938.

(19) Rica, R.; Ziano, R.; Salerno, D.; Mantegazza, F.; Brogioli, D. Thermodynamic relation between voltage-concentration dependence and salt adsorption in electrochemical cells. *Phys. Rev. Lett.* **2012**, *109* (15), 156103.

(20) Rica, R. A.; Ziano, R.; Salerno, D.; Mantegazza, F.; Bazant, M. Z.; Brogioli, D. Electro-diffusion of ions in porous electrodes for capacitive extraction of renewable energy from salinity differences. *Electrochim. Acta* **2013**, *92* (0), 304−314.

(21) Iglesias, G. R.; Fernández, M. M.; Ahualli, S.; Jiménez, M. L.; Kozynchenko, O. P.; Delgado, Á. V. Materials selection for optimum energy production by double layer expansion methods. *J. Power Sources* **2014**, *261*, 371−377.

(22) Porada, S.; Zhao, R.; Van Der Wal, A.; Presser, V.; Biesheuvel, P. Review on the science and technology of water desalination by capacitive deionization. *Prog. Mater. Sci.* **2013**, *58* (8), 1388−1442.

(23) Biesheuvel, P. Thermodynamic cycle analysis for capacitive deionization. *J. Colloid Interface Sci.* **2009**, *332* (1), 258−264.

(24) Anderson, M. A.; Cudero, A. L.; Palma, J. Capacitive deionization as an electrochemical means of saving energy and delivering clean water. Comparison to present desalination practices: Will it compete? *Electrochim. Acta* **2010**, *55* (12), 3845−3856.
(25) Hatzell, K. B.; Iwama, E.; Ferris, A.; Daffos, B.; Urita, K.; Tzedakis, T.; Chauvet, F.; Taberna, P.-L.; Gogotsi, Y.; Simon, P. Capacitive deionization concept based on suspension electrodes without ion exchange membranes. *Electrochem. Commun.* **2014**, *43*, 18−21.
(26) Suss, M. E.; Baumann, T. F.; Bourcier, W. L.; Spadaccini, C. M.; Rose, K. A.; Santiago, J. G.; Stadermann, M. Capacitive desalination with flow-through electrodes. *Energy Environ. Sci.* **2012**, *5* (11), 9511−9519.
(27) Sales, B. B.; Saakes, M.; Post, J. W.; Buisman, C. J. N.; Biesheuvel, P. M.; Hamelers, H. V. M. , Direct power production from a water salinity difference in a membrane-modified supercapacitor flow cell. *Environ. Sci. Technol.* **2010**, *44* (14), 5661−5665.
(28) Hatzell, M. C.; Cusick, R. D.; Logan, B. Capacitive mixing power production from salinity gradient energy enhanced through exoelectrogen-generated ionic currents. *Energy Environ. Sci.* **2014**, *7*, 1159−1165.
(29) Watson, V. J.; Nieto Delgado, C.; Logan, B. E. Influence of chemical and physical properties of activated carbon powders on oxygen reduction and microbial fuel cell performance. *Environ. Sci. Technol.* **2013**, *47*, 6704−6710.
(30) te Velde, G.; Bickelhaupt, F. M.; Baerends, E. J.; Fonseca Guerra, C.; van Gisbergen, S. J. A.; Snijders, J. G.; Ziegler, T. Chemistry with ADF. *J. Comput. Chem.* **2001**, *22* (9), 931−967.
(31) van Duin, A. C. T.; Dasgupta, S.; Lorant, F.; Goddard, W. A. ReaxFF: A reactive force field for hydrocarbons. *J. Phys. Chem. A* **2001**, *105* (41), 9396−9409.
(32) Chenoweth, K.; van Duin, A. C. T.; Goddard, W. A. ReaxFF reactive force field for molecular dynamics simulations of hydrocarbon oxidation. *J. Phys. Chem. A* **2008**, *112* (5), 1040−1053.
(33) Bagri, A.; Mattevi, C.; Acik, M.; Chabal, Y. J.; Chhowalla, M.; Shenoy, V. B. Structural evolution during the reduction of chemically derived graphene oxide. *Nat. Chem.* **2010**, *2* (7), 581−587.
(34) Rahaman, O.; van Duin, A. C. T.; Goddard, W. A.; Doren, D. J. Development of a ReaxFF reactive force field for glycine and application to solvent effect and tautomerization. *J. Phys. Chem. B* **2010**, *115* (2), 249−261.
(35) Rahaman, O.; van Duin, A. C. T.; Bryantsev, V. S.; Mueller, J. E.; Solares, S. D.; Goddard, W. A.; Doren, D. J. Development of a ReaxFF reactive force field for aqueous chloride and copper chloride. *J. Phys. Chem. A* **2010**, *114* (10), 3556−3568.
(36) Bonomi, M.; Branduardi, D.; Bussi, G.; Camilloni, C.; Provasi, D.; Raiteri, P.; Donadio, D.; Marinelli, F.; Pietrucci, F.; Broglia, R. A.; Parrinello, M. PLUMED: A portable plugin for free-energy calculations with molecular dynamics. *Comput. Phys. Commun.* **2009**, *180* (10), 1961−1972.
(37) Goldberg, S. *Surface Complexation Modeling*; USDA-ASR: Riverside, CA, 2013.
(38) Noh, J. S.; Schwarz, J. A. Effect of HNO_3 treatment on the surface acidity of activated carbons. *Carbon* **1990**, *28* (5), 675−682.
(39) Hulicova-Jurcakova, D.; Seredych, M.; Lu, G. Q.; Bandosz, T. J. Combined effect of nitrogen-and oxygen-containing functional groups of microporous activated carbon on its electrochemical performance in supercapacitors. *Adv. Funct. Mater.* **2009**, *19* (3), 438−447.
(40) Petersen, M. K.; Kumar, R.; White, H. S.; Voth, G. A. A computationally efficient treatment of polarizable electrochemical cells held at a constant potential. *J. Phys. Chem. C* **2012**, *116* (7), 4903−4912.